Sun, Kewei; Krejci, Ondrej; Foster, Adam S.; Okuda, Yasuhiro; Orita, Akihiro; Kawai, Shigeki

Synthesis of Regioisomeric Graphene Nanoribbon Junctions via Heteroprecursors

Published in:
Journal of Physical Chemistry C

DOI:
10.1021/acs.jpcc.9b05881

Published: 18/07/2019

Document Version
Peer-reviewed accepted author manuscript, also known as Final accepted manuscript or Post-print

Please cite the original version:
Sun, K., Krejci, O., Foster, A. S., Okuda, Y., Orita, A., & Kawai, S. (2019). Synthesis of Regioisomeric Graphene Nanoribbon Junctions via Heteroprecursors. *Journal of Physical Chemistry C*, *123*(28), 17632-17638. https://doi.org/10.1021/acs.jpcc.9b05881

Synthesis of Regioisomeric Graphene Nanoribbon Junctions *via* Hetero Precursors

*Kewei Sun[1], Ondřej Krejčí[2], Adam S. Foster[2,3,4], Yasuhiro Okuda[5], Akihiro Orita[5], Shigeki Kawai[1]**

[1]*International Center for Materials Nanoarchitectonics, National Institute for Materials Science, 1-1 Namiki, Tsukuba, Ibaraki 305-0044, Japan*

[2]*Department of Applied Physics, Aalto University School of Science, P.O. Box 11100, FI-00076 Aalto, Finland.*

[3]*WPI Nano Life Science Institute (WPI-NanoLSI), Kanazawa University, Kakuma-machi, Kanazawa 920-1192, Japan.*

[4]*Graduate School Materials Science in Mainz, Staudinger Weg 9, 55128, Germany*

[5]*Department of Applied Chemistry and Biotechnology, Okayama University of Science, 1-1 Ridai-cho, Kita-ku, Okayama, 700-0005, Japan.*

ABSTRACT: Graphene nanoribbons are one of the most promising materials for nanoscale electronics. While various structures have successfully been synthesized by on-surface reaction, curved connections remain less investigated, yet they could prove highly useful in the development of copolymerization technology. Here, we present the synthesis of three different regioisomeric junctions on Au (111) by using 10,10'-dibromo-9,9'-bianthryl and 1,3,6,8-tetrabromopyrene. The

chemical structures and the electronic properties of junctions were studied with a combination of scanning tunneling microscopy with a CO terminated tip, scanning tunneling spectroscopy, and density functional theory calculations. We found that two identical nanoribbon-junction interface electronic states appear within the band gaps of connected graphene nanoribbons.

1. INTRODUCTION

Quasi-one dimensional graphene nanoribbons (GNRs) are considered as fundamental components for future carbon-based electronic devices due to their controllable electronic structure, which can be tuned by changing the ribbon width and edge structure. The so-called top-down approach, via the cutting of graphene and opening of carbon nanotubes, has demonstrated the possibilities of obtaining nanometer-sized GNRs.[1,2] However, it is quite challenging to control their widths and edge structures at the atomic-scale. In order to overcome this issue, a bottom-up approach, via on-surface synthesis, has been developed.[3] In this technique, small molecules substituted by two halogen atoms are used as precursors. They are deposited on noble metal surfaces, then annealed to cleave the C-X (X=Cl, Br, I) bonds and the resulting radicals then diffuse on the surface until stabilization by the formation of a C-C bond.[3] Further annealing at higher temperatures induces the dehydrogenation of the polymerized chains, resulting in the formation of GNRs.[4] With appropriate precursors, various GNRs with given structures have been synthesized, such as armchair edge GNRs with different widths,[5-11] chevron GNRs,[5] zigzag edge GNRs,[12] cove-edged GNRs,[13] chiral GNRs,[14-17] porous GNRs,[18] and doped GNRs (B, N, O, S)[19-26] as well as the *p-n* and hetero-junctions of GNRs.[27-33] Among all the precursors, 10,10'-dibromo-9,9'-bianthryl (DBBA) is the mostly used even on different metal surfaces.[34-36]For the future development of reliable electronic devices, it is of central importance to control the structure of junctions and investigate their electronic properties.[27-33,37,38] Yet, structurally defined junctions between GNRs by a hetero molecule has not been demonstrated.

Here, we present the structural junctions of n=7 armchair edge GNRs (n: the number of carbon in width), atomically defined by the backbone of 1,3,6,8-tetrabromopyrene (TBP) through on-surface chemical reaction. When TBP was treated with DBBA on Au (111), TBP reacted with

DBBA at two bromine sites out of four to give three different regioisomeric GNR junctions. Scanning tunneling microscopy (STM) with a CO functionalized tip shows the detailed structures of junctions. Furthermore, scanning tunneling spectroscopy (STS) revealed two local electronic states in the band gap of connected GNRs around the junction interface for each type of junction. Density functional theory (DFT) calculations also demonstrate the presence and character of these interface states. We propose that patterning GNR with regioisomeric junctions can lead to alternation of electronic properties of GNR.

2. METHODS

STM Measurements. All measurements were performed with a home-made low temperature tunneling microscopy (STM)/atomic force microscopy system, operating in ultrahigh vacuum at 4.3 K. The samples were prepared in an ultra-high vacuum environment ($<5\times10^{-10}$ mbar). Au (111) surfaces were cleaned through cyclic sputtering (Ar^+, 10 minutes) and annealing (750 K, 10 minutes). 10,10'-dibromo-9,9'-bianthryl (DBBA, Sigma-Aldrich) and 1,3,6,8-tetrabromopyrene (TBP)[39] molecules were deposited with a ratio of DBBA to TBP as 10:1 onto the Au (111) surface held at room temperature. Then the samples were heated to 180 ℃ (15 minutes) and 320 ℃ (15 minutes) for dehalogenation and cyclodehydrogenation, respectively. The temperature of sample was measured by a thermocouple and a pyrometer. A chemically etched tungsten tip was employed as a probe. For high-resolution imaging, the tip apex was terminated with a CO molecule, which was picked up from the surface[40]. The number of membered ring was determined by counting the number of the neighboring rings as well as a void in the observed image. For constant height dI/dV imaging. the sample bias voltage was set close to zero voltage. The modulation amplitude was 7

mV_{rms} and the frequency was 510 Hz. The WSxM software was used to analyze all measured images.[41]

Theoretical Calculations. All first principles calculations in this work were performed using the periodic plane-wave basis VASP code[42,43] implementing the spin-polarized density functional theory (DFT). To accurately include van der Waals interactions in this system we used the optB86B+vdW-DF functional,[44,45] selected based on previous work showing that it provides a sufficiently accurate description for all subsystems involved in the measurement. For similar systems,[23] this has given comparable accuracy in adsorbed molecular structures to vdW functionals D3[46] and TS.[47] For hybrid functional calculations we used the HSE06 functional[48,49] along with the D3 method to include vdW contributions.[46]

Projected augmented wave (PAW) potentials were used to describe the core electrons,[50] with a kinetic energy cutoff of 550 eV (with PREC=accurate). Systematic k-point convergence was checked for all systems, with sampling chosen according to system size. This approach converged the total energy of all the systems to the order of meV. The properties of the bulk and surface of Au were carefully checked within this methodology, and excellent agreement was achieved with experiments. For calculations of the GNR junctions and GNR junctions on the surface, a vacuum gap of at least 1.5 nm was used, and the upper three layers of Au (five layers in total) and all atoms in the junction were allowed to relax to a force of less than 0.01 eV/Angström.

For calculations of the *trans* junction, the size of junction unit matched well to a gold supercell, but for the cis_1 junction, the junction was by reduced by 2 % to find a reasonable match with gold. A comparison of the electronic structure of the original and reduced cis_1 junction electronic structure showed no significant differences. STM images were calculated using the HIVE package

[51] based on the Tersoff-Hamann approximation.[52] Atomic structure visualizations were made with the VMD package.[53]

3. RESULTS AND DISCUSSION

We employ two kinds of precursor molecules (DBBA and TBP) to fabricate junctions (Scheme 1). If a small amount of TBP molecules are co-deposited, DBBA molecules are expected to covalently connect to one of the four bromo-substituted sites in TBP via an Ullmann-type reaction. This conjugation repeats with DBBAs, resulting in the growth of a polyanthrylene attached to the pyrene core. Since TBP has four bromo-substituted sites, the position and the number of the polyanthrylene unit can vary. To simplify the discussion, here we focus on junctions in which two polyanthrylene units link to one TBP. Subsequently, the cyclodehydrogenation induced by high-temperature annealing leads to the formation of a junction connecting two n=7 GNRs. The angles between the GNRs at the junction, 180°, ~60° and ~120° (see Scheme 1), define three types of regioisomeric junction, one *trans* and two *cis* forms respectively.

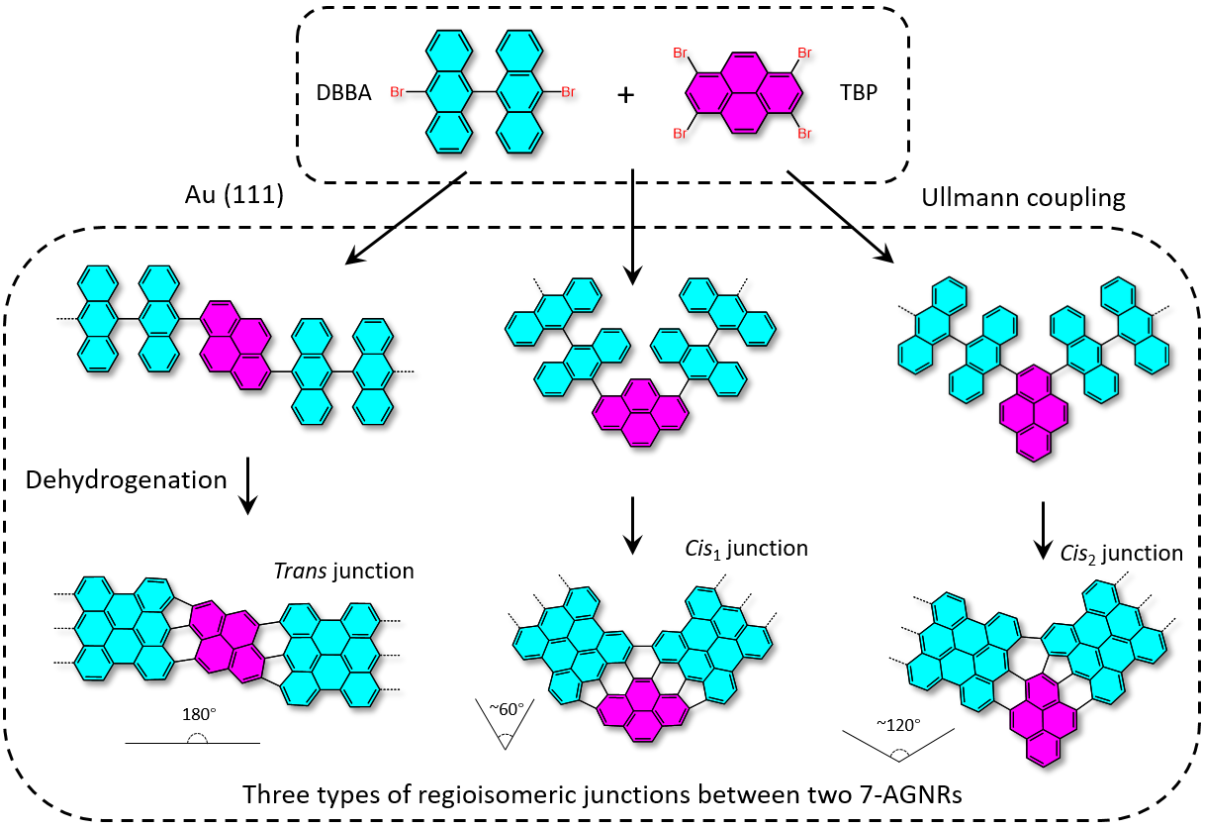

Scheme 1. Reaction processes to form three types of regioisomeric junctions between two graphene nanoribbons.

Based on this scenario, we investigated reaction conditions for the construction of bis(polyanthrylene)-substituted pyrene as a major junction in on-surface polymerization. Fortunately, we found that when DBBA and TBP were deposited with a ratio of 10:1 onto a Au (111) surface at room temperature and heated at 180 °C, Ullmann couplings for DBBA-TPB conjugation as well as for DBBA-polymerization proceeded smoothly to give the desired bis(polyanthrylene)-substituted pyrenes. Subsequently, the substrate was annealed at 320 °C to induce cyclodehydrogenation. Figure 1a shows the STM topography, in which a nodal site between two GNRs can be seen as indicated by a yellow dashed box. To investigate the structure in detail, the tip apex was terminated by a CO molecule.[54,55] The lateral flexibility of the CO molecule on

the metal tip ensures resolution of the inner structures of molecules on surfaces directly.[56] Figure 1b shows the detailed structure, in which two GNRs are connected with a small offset along the longitudinal axis. At the center of the junction, four fused six-membered rings, corresponding to a pyrene core derived from TBP, can be seen. Therefore, the GNR is conjugated to TBP via one pair of five and six membered rings. This structure corresponds to a *trans* junction (Scheme 1). Note that the junction is chiral (Figure S1) and composed of zig-zag edges.

We also found two types of *cis* junctions, which have both V-shaped structures. Figure 1c shows the STM topography of the junction with a narrower opening angle. Since the measured angle is about 60°, suggesting it corresponds to a cis_1 junction. Indeed, the high-resolution dI/dV image shows the chemical structure in which two GNRs are connected symmetrically via TBP (Figure 1d). Figure 1e shows a closeup view of the junction in which two five-membered rings are indicated in red. Therefore, the GNR is connected to a TBP with one pair of five- and six-membered rings. Furthermore, a narrow gap between two GNRs results in the formation of a six-membered ring at the inner corner. From this investigation, it can be concluded that the structure corresponds to the cis_1 junction.

Figure 1f shows another example with a wider opening angle of ~120°. A high-resolution dI/dV image taken around the area indicated by a dashed box in figure 1f gives the detailed chemical structure (Figure 1g). The structure of the junction is not line symmetric as the GNR on the left-hand side is closer to the horizontal line of image compared to the right-hand side. Figure 1h shows a closeup view of the junction, in which asymmetric connections can clearly be seen. The GNR on the left-hand side connects to the TBP via one pair of six- and seven-membered rings, while the GNR on the right-hand side connects via one pair of five- and six-membered rings, matching the cis_2 junction (see Scheme 1). While we observed three types of junction between two

GNRs, junctions among three or four GNRs were not observed. It may be due to the fact that the steric effect between GNRs prevents the Ullmann-type reaction. On the other hand, one GNR terminated by TBP was observed (Figure S2). Note that observed junctions that are not defined by the backbone of TBP, may relate to a random fusion of GNRs due to a low purity of the employed DBBA or C-H activation of zigzag terminal of GNRs, as such junctions could also be seen without a TBP molecule (Figure S3).

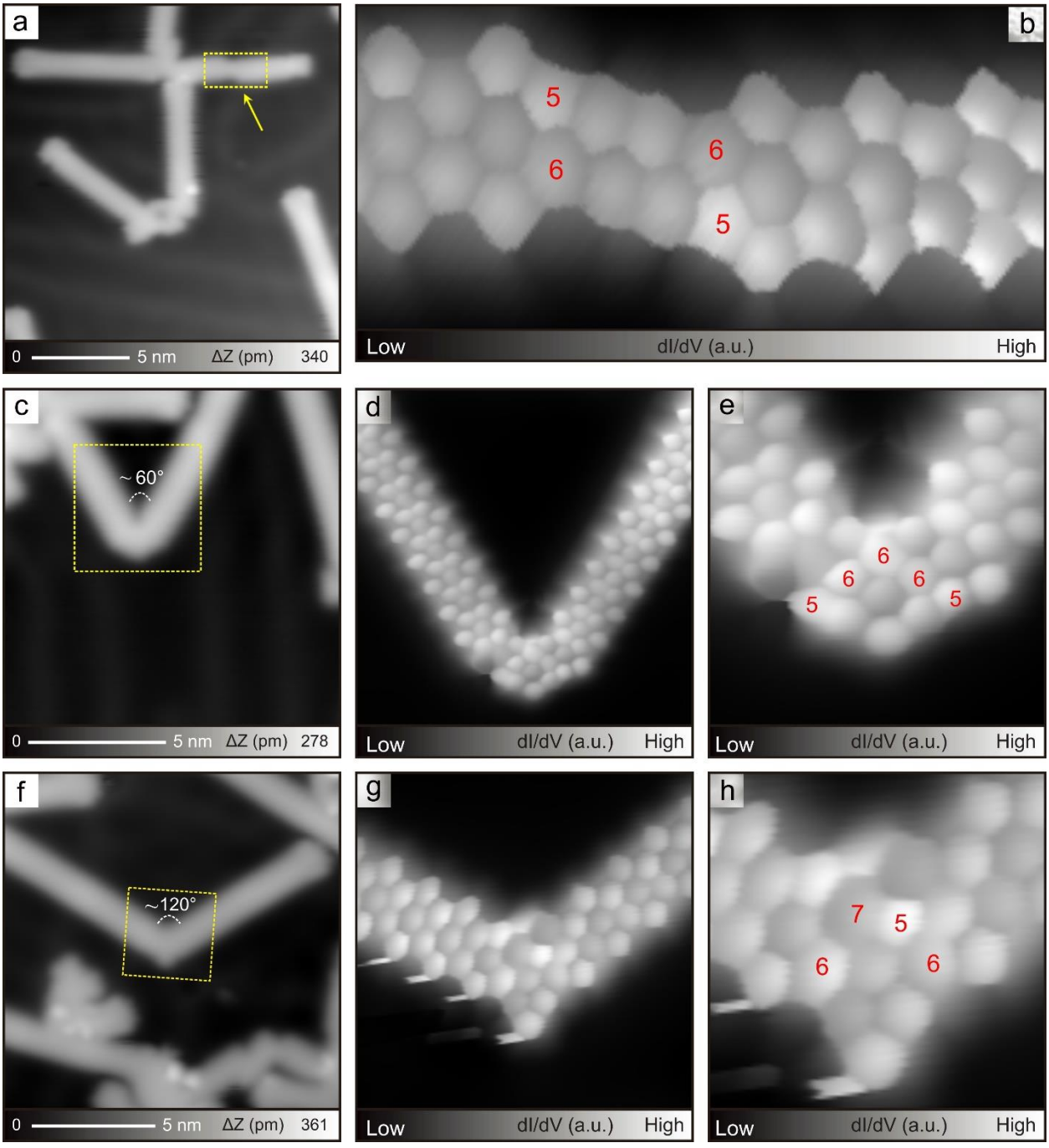

Figure 1. Three types of regioisomeric junctions synthesized on Au (111). (a) STM topography of a straight junction with a nodal site indicated by a yellow arrow. (b) CO terminated tip constant height d*I*/d*V* image of the area marked by a dashed box in (a). (c) STM topography of V-shaped junction with an angle of ~60°. (d) Constant height d*I*/d*V* image of the area marked by a dashed

box in (c) and its closeup view in (e). (f) STM topography of the V-shaped structure with an angle of ~120°. (g) Constant height dI/dV image of the area marked by a dashed box in (f) and its closeup view in (h). Measurement parameters: Sample bias voltage V = 200 mV and tunneling current I = 10 pA in (a) and (f). V = 200 mV and I = 5 pA in (c).

Next, we investigated the electronic structures of the junctions by STS measurement. Figure 2a shows the STM topography of a *trans* junction on Au (111). The dI/dV curves were recorded above three different sites (Figure 2b), at the interface of the junction (indicated by a blue cross), at the bulk of the GNR connected junction (indicated by a red cross) and at the bare Au (111) surface as a reference. The characteristic surface state of Au (111) at ~-0.5 V is also visible in the dI/dV curves taken above the GNR and *trans* junction. Although the GNRs connect to the junction, no significant change of the valence band (VB) state (-0.8 V) and the conduction band (CB) state (+1.7 V) is observed above the GNR, remaining similar to an isolated GNR on Au(111).[57] Besides the VB and CB states, two additional peaks at -0.6 V and +1.0 V, marked by black arrows in figure 2b, within the band gap of GNR can be identified. In order to investigate the spatial distribution of the electronic states, we took dI/dV maps at characteristic energies. Figures 2c and f show the dI/dV maps at bias voltages of -0.8 V and 1.7 V, respectively. The two additional peaks localize only in the close vicinity of the junction and disappear rapidly with the distance.

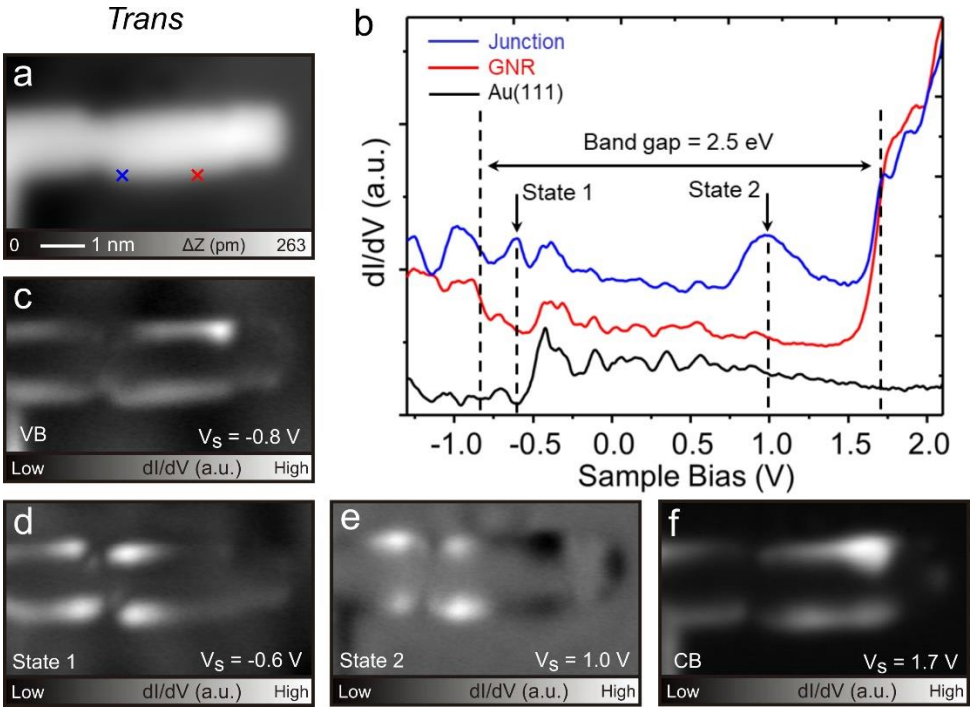

Figure 2. STS measurement of the *trans* junction. (a) STM topography of a *trans* junction on Au (111). (b) d*I*/d*V* curves were recorded at the junction (blue line) and bulk of GNR (red line) as well as Au (111) surface (black line). (c-f) A series of constant current d*I*/d*V* images were obtained at different sample bias voltages. Measurement parameters: $V = 200$ mV, $I = 10$ pA.

We also carried out STS measurement above two different sites of the cis_1 junction, indicated by crosses in figure 3a. Figure 3b shows the corresponding dI/dV curves, and again, two additional peaks were measured at -0.42 V and 1.0 V only above the junction (Figure 3b). Figures 3c and f show that the VB and CB states of connected GNRs are distributed at the ribbon edges. The two interface states (-0.42 V and 1.0 V) also localize in the vicinity of the cis_1 junction (Figures 3d and e), similar to the case of the *trans* junction. The electronic structure of the cis_2 junction was also investigated. The results can be seen in figure S4, where two interface states (-0.56 V and 0.87 V) are almost the same as those in *trans* and cis_1 junctions.

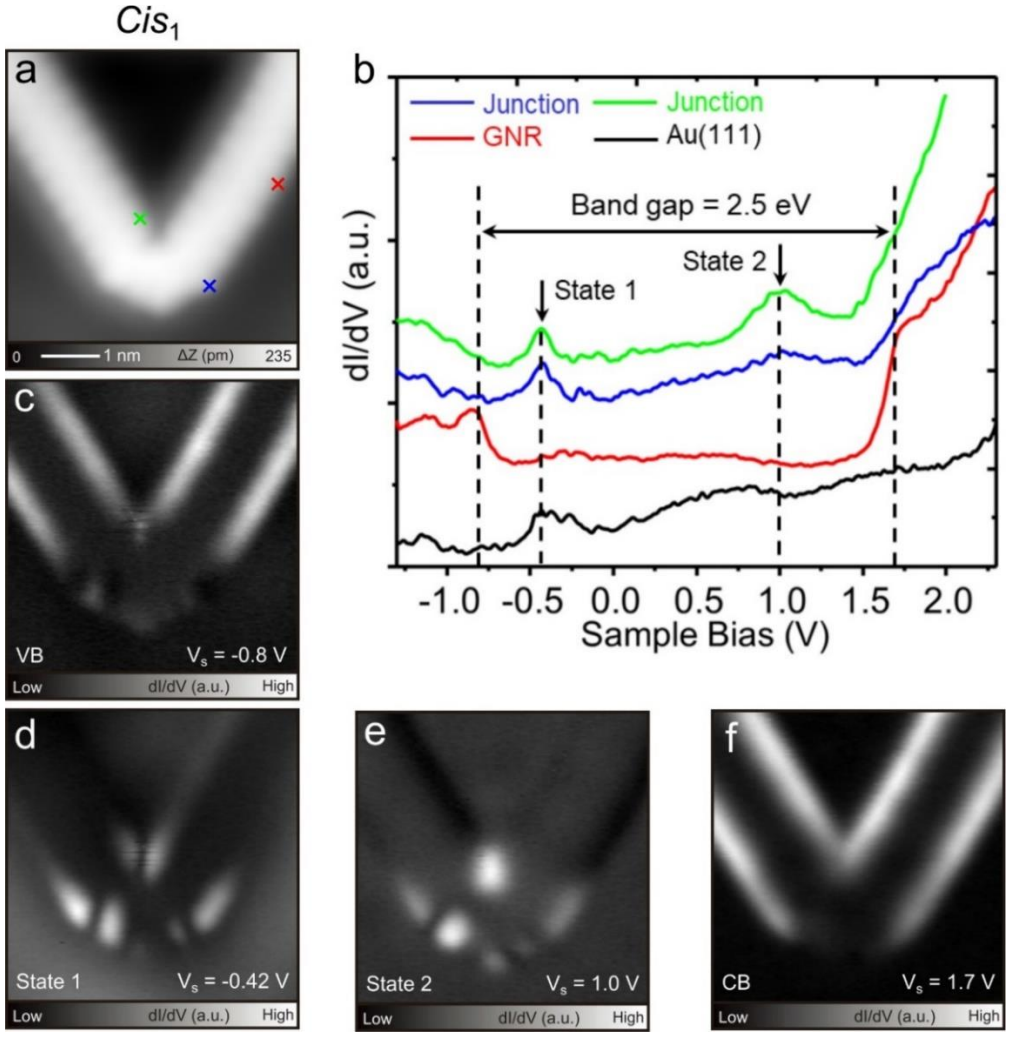

Figure 3. STS measurement of the *cis*$_1$ junction. (a) STM topography of *cis*$_1$ junction on Au (111). (b) d*I*/d*V* curves were recorded at the junction (blue and green lines), bulk of GNR (red line) and Au (111) surface (black line). (c-f) A series of constant current d*I*/d*V* images were carried out at different bias voltages. Measurement parameters: $V = 200$ mV, $I = 10$ pA.

Three different junctions have been all synthesized through a single TBP molecule connecting terminals of two GNRs. Each of them introduce two localized states around the interfaces of junctions. This is of particular interest, since interface states have the potential to tune

the electronic properties of GNRs. For example, a periodic junction structure may introduce an interface state throughout the whole structure, resulting into a new band gap. Moreover, some periodic GNR junctions even have topological character. [58-60]

In order to understand the origin and character of the observed interface states, we performed DFT calculations to study the atomic and electronic structure of the junctions. Since the observed properties were very similar for all the junctions considered, we focus here on the *trans* and cis_1 junctions. In figure 4b, simulations demonstrate a clear presence of the state in the gap of GNR at about 0.5 eV and a further state at the top of valence band at -0.5 eV. Calculated dI/dV maps at those energies (Figure 4c) show that they are dominated by states near the junction, and show reasonable agreement with the equivalent experimental images (Figure 2). A more detailed analysis of the atomic character dominating states at those energies supports this, with carbon atoms around the junction playing a leading role (Figure S6).

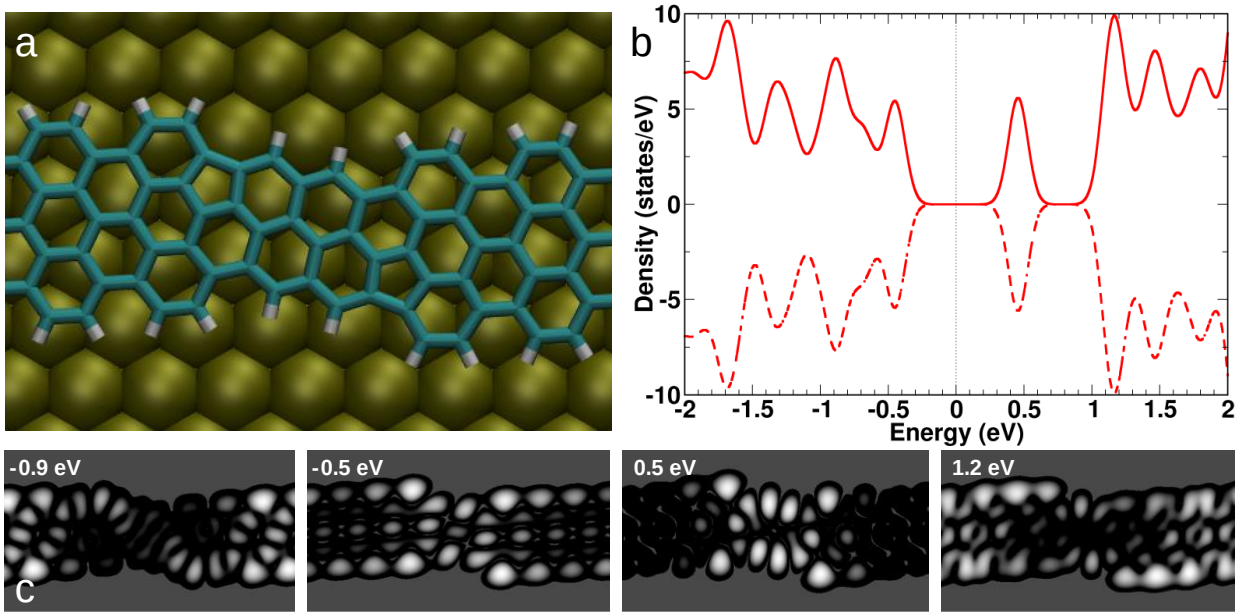

Figure 4. Simulated properties of *trans* junction: (a) atomic structure, (b) Density of States around the Fermi energy where the solid line is spin *up* and dashed spin *down,* and (c) calculated d*I*/d*V* at a height of 0.3 nm above the junction and at the energies given.

Equivalently for the *cis*$_1$ junction, figure 5b shows two clear states split off from the main GNR bands at about ±0.3 eV, with characteristic features seen in the experimental d*I*/d*V* images (Figure 3) reproduced in the calculated maps (Figure 5c). As for the *trans* junction, these states are clearly dominated in character by carbon atoms at the junction (Figure S8).

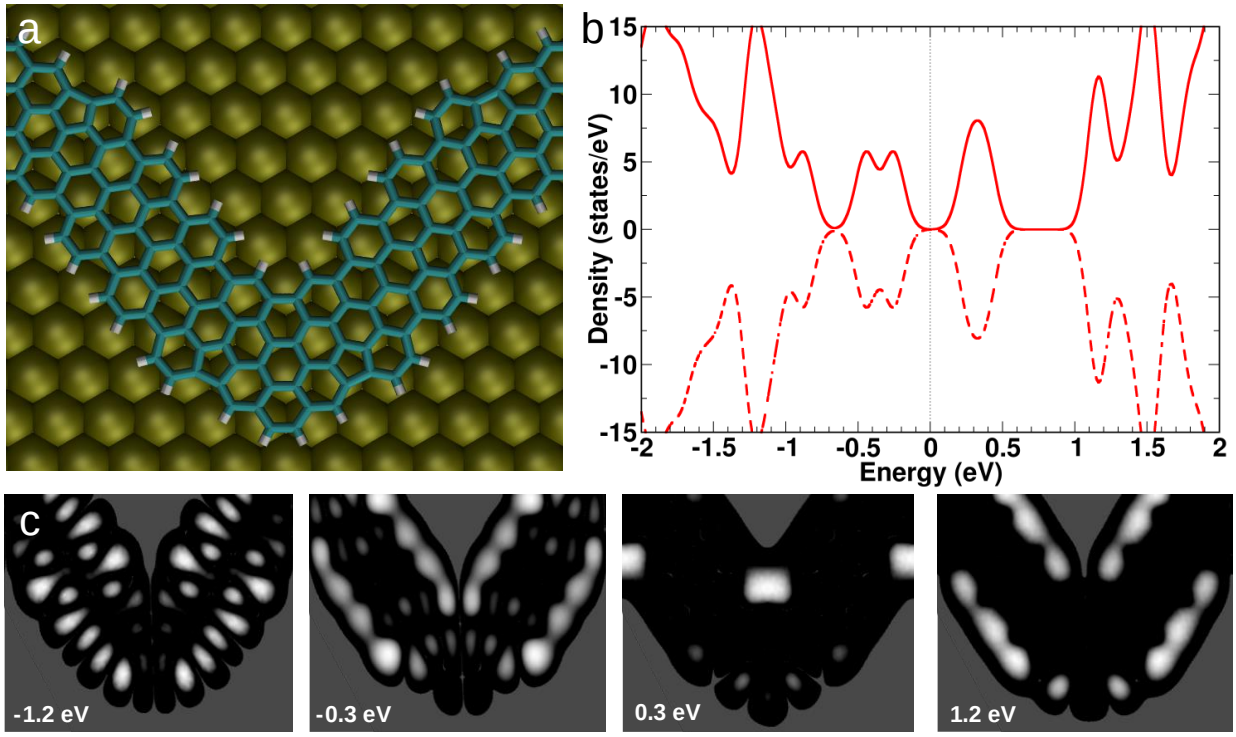

Figure 5: Simulated properties of *cis*$_1$ junction: (a) atomic structure, (b) Density of States around the Fermi energy where the solid line is spin *up* and dashed spin *down,* and (c) calculated d*I*/d*V* at a height of 0.3 nm above the junction and at the energies given.

Note that the electronic structure analysis presented in figure 5 and 6 is based on isolated periodic junctions without the substrate for clarity, but we also simulated the same structures on a

gold surface and obtained very similar results (see Figures S5-8). Calculations of the junctions with hybrid functionals also demonstrated that the electronic structure is qualitatively the same and the interface states persist (see Figures S5 and S7).

4. CONCLUSIONS

By employing two hetero precursor molecules, we have synthesized the structure of regioisomeric junctions between two n=7 graphene nanoribbons by the backbone of a TBP molecule at the atomic-scale. Since TBP has four Br substations, three possible connections were expected. Indeed, we found all three and characterized them by high-resolution STM and STS. GNRs and TBP molecules are conjugated with each other *via* five-, six-, and seven-membered rings, depending on the fused positions of the TBP. In contrast, the electronic structures of the three different junctions were almost identical. For all the types, the nature of the effective *defects* creating the junctions means that the two interface states localize in their close vicinity. Since this technique offers a possibility to fabricate the structure of the junctions between GNRs, various junctions can be potentially synthesized. Thus, this finding may be a useful step forward towards carbon-based nanoelectronics.

ASSOCIATED CONTENT

Supporting Information

The Supporting Information is available free of charge on the ACS Publications website at DOI:.

STM images of chiral *trans* junctions, 7-AGNR terminated by one TBP or 7-AGNR, STS measurement of the cis_2 junction, Simulated properties of *trans* and cis_1 junctions on the gold surface (PDF).

AUTHOR INFORMATION

Corresponding Author

* KAWAI.Shigeki@nims.go.jp

Notes

Any additional relevant notes should be placed here.

ACKNOWLEDGEMENTS

This work was supported in part by Japan Society for the Promotion of Science (JSPS) KAKENHI Grant Number 15K21765 and 19H00856 to S.K., JP18H04430 in Middle Molecular Strategy and JP18K05134 to A.O., JP19K15574 to Y.O., Okayama Prefecture Industrial Promotion Foundation (A.O.), Okayama Foundation of Science and Technology (Y.O.), Promotion and Mutual Aid Corporation for Private Schools of Japan (Y. O.) and OUS Research Project (OUS-RP-19-4 to A. O. and Y.O.). The authors (A.O. and Y.O.) thank to Research Instruments Center, Okayama University for the measurements of 300 MHz NMR (LA300), 400 MHz NMR (JNM-ECS400 and JNM-ECZ400) and MALDI-TOF MS measurements. Computing resources from the Aalto Science-IT project and CSC, Helsinki are gratefully acknowledged. ASF has been supported by the World Premier International Research Center Initiative (WPI), MEXT, Japan. S.K. sincerely

thank Ernst Meyer, Urs Gysin, Sascha Martin, and Yves Pellmont for support to build the microscope.

REFERENCES

1. Li, X. L.; Wang, X. R.; Zhang, L.; Lee, S. W.; Dai, H. J. Chemically Derived, Ultrasmooth Graphene Nanoribbon Semiconductors. *Science* **2008**, *319*, 1229−1232.
2. Kosynkin, D. V.; Higginbotham, A. L.; Sinitskii, A.; Lomeda, J. R.; Dimiev, A.; Price, B. K.; Tour, J. M. Longitudinal Unzipping of Carbon Nanotubes to Form Graphene Nanoribbons. *Nature* **2009**, *458*, 872−876.
3. Grill, L.; Dyer, M.; Lafferentz, L.; Persson, M.; Peters, M. V.; Hecht, S. Nano-Architectures by Covalent Assembly of Molecular Building Blocks. *Nat. Nanotechnol.* **2007**, *2*, 687−691.
4. Talirz, L.; Ruffieux, P.; Fasel, R. On-Surface Synthesis of Atomically Precise Graphene Nanoribbons. *Adv. Mater.* **2016**, *28*, 6222−6231.
5. Cai, J.; Ruffieux, P.; Jaafar, R.; Bieri, M.; Braun, T.; Blankenburg, S.; Muoth, M.; Seitsonen, A. P.; Saleh, M.; Feng, X.; et al. Atomically Precise Bottom-Up Fabrication of Graphene Nanoribbons. *Nature* **2010**, *466*, 470−473.
6. Chen, Y.-C.; de Oteyza, D. G.; Pedramrazi, Z.; Chen, C.; Fischer, F. R.; Crommie, M. F. Tuning the Band Gap of Graphene Nanoribbons Synthesized from Molecular Precursors. *ACS Nano* **2013**, *7*, 6123−6128.
7. Zhang, H.; Lin, H.; Sun, K.; Chen, L.; Zagranyarski, Y.; Aghdassi, N.; Duhm, S.; Li, Q.; Zhong, D.; Li, Y.; et al. On-Surface Synthesis of Rylene-Type Graphene Nanoribbons. *J. Am. Chem. Soc.* **2015**, *137*, 4022−4025.

8. Kimouche, A.; Ervasti, M. M.; Drost, R.; Halonen, S.; Harju, A.; Joensuu, P. M.; Sainio, J.; Liljeroth, P. Ultra-Narrow Metallic Armchair Graphene Nanoribbons. *Nat. Commun.* **2015**, *6*, 10177.
9. Basagni, A.; Sedona, F.; Pignedoli, C. A.; Cattelan, M.; Nicolas, L.; Casarin, M.; Sambi, M. Molecules−Oligomers−Nanowires−Graphene Nanoribbons: A Bottom-Up Stepwise On-Surface Covalent Synthesis Preserving Long-Range Order. *J. Am. Chem. Soc.* **2015**, *137*, 1802−1808.
10. Talirz, L.; Söde, H.; Dumslaff, T.; Wang, S.; Sanchez-Valencia, J. R.; Liu, J.; Shinde, P.; Pignedoli, C. A.; Liang, L.; Meunier, V.; et al. On-Surface Synthesis and Characterization of 9-atom Wide Armchair Graphene Nanoribbons. *ACS Nano* **2017**, *11*, 1380−1388.
11. Abdurakhmanova, N.; Amsharov, N.; Stepanow, S.; Jansen, M.; Kern, K.; Amsharov, K. Synthesis of Wide Atomically Precise Graphene Nanoribbons from Para-oligophenylene Based Molecular Precursor. *Carbon* **2014**, *77*, 1187−1190.
12. Ruffieux, P.; Wang, S.; Yang, B.; Sánchez-Sánchez, C.; Liu, J.; Dienel, T.; Talirz, L.; Shinde, P.; Pignedoli, C. A.; Passerone, D.; Dumslaff, T.; Feng, X.; Müllen, K.; Fasel, R. On-Surface Synthesis of Graphene Nanoribbons with Zigzag Edge Topology. *Nature* **2016**, *531*, 489−492.
13. Liu, J.; Li, B. W.; Tan, Y. Z.; Giannakopoulos, A.; Sanchez-Sanchez, C.; Beljonne, D.; Ruffieux, P.; Fasel, R.; Feng, X.; Müllen, K. Toward Cove-Edged Low Band Gap Graphene Nanoribbons. *J. Am. Chem. Soc.* **2015**, *137*, 6097−6103.
14. Han, P.; Akagi, K.; Canova, F.; Mutoh, H.; Shiraki, S.; Iwaya, K.; Weiss, P.; Asao, N.; Hitosugi, T. Bottom-up Graphene-Nanoribbon Fabrication Reveals Chiral Edges and Enantioselectivity. *ACS Nano* **2014**, *8*, 9181−9187.

15. Sánchez-Sánchez, C.; Dienel, T.; Deniz, O.; Ruffieux, P.; Berger, R.; Feng, X.; Müllen, K.; Fasel, R. Purely Armchair or Partially Chiral: Noncontact Atomic Force Microscopy Characterization of Dibromo-Bianthryl-Based Graphene Nanoribbons Grown on Cu(111). *ACS Nano* **2016**, *10*, 8006−8011.
16. de Oteyza, D. G.; García-Lekue, A.; Vilas-Varela, M.; Merino-Díez, N.; Carbonell-Sanromà, E.; Corso, M.; Vasseur, G.; Rogero, C.; Guitián, E.; Pascual, J. I.; et al. Substrate-Independent Growth of Atomically Precise Chiral Graphene Nanoribbons. *ACS Nano* **2016**, *10*, 9000−9008.
17. Wang, X. Y.; Urgel, J. I.; Barin, G. B.; Eimre, K.; Di Giovannantonio, M.; Milani, A.; Tommasini, M.; Pignedoli, C. A.; Ruffieux, P.; Feng, X.; et al. Bottom-up Synthesis of Heteroatom-Doped Chiral Graphene Nanoribbons. *J. Am. Chem. Soc.* **2018**, *140*, 9104−9107.
18. Moreno, C.; Vilas-Varela, M.; Kretz, B.; Garcia-Lekue, A.; Costache, M. V.; Paradinas, M.; Panighe, M.; Ceballos, G.; Valenzuela, S. O.; Peña, D.; et al. Bottom-Up Synthesis of Multifunctional Nanoporous Graphene. *Science* **2018**, *360*, 199−203.
19. Bronner, C.; Stremlau, S.; Gille, M.; Brausse, F.; Haase, A.; Hecht, S.; Tegeder, P. Aligning the Band Gap of Graphene Nanoribbons by Monomer Doping. *Angew. Chem. Int. Ed.* **2013**, *52*, 4422−4425.
20. Zhang, Y.; Zhang, Y.; Li, G.; Lu, J.; Lin, X.; Du, S.; Berger, R.; Feng, X.; Müllen, K.; Gao, H.-J. Direct Visualization of Atomically Precise Nitrogen-Doped Graphene Nanoribbons. *Appl. Phys. Lett.* **2014**, *105*, 023101.

21. Kawai, S.; Saito, S.; Osumi, S.; Yamaguchi, S.; Foster, A. S.; Spijker, P.; Meyer, E. Atomically Controlled Substitutional Boron-Doping of Graphene Nanoribbons. *Nat. Commun.* **2015**, *6*, 8098.

22. Cloke, R. R.; Marangoni, T.; Nguyen, G. D.; Joshi, T.; Rizzo, D. J.; Bronner, C.; Cao, T.; Louie, S. G.; Crommie, M. F.; Fischer, F. R. Site-Specific Substitutional Boron Doping of Semiconducting Armchair Graphene Nanoribbons. *J. Am. Chem. Soc.* **2015**, *137*, 8872−8875.

23. Kawai, S.; Nakatsuka, S.; Hatakeyama, T.; Pawlak, R.; Meier, T.; Tracey, J.; Meyer, E.; Foster, A. S. Multiple Heteroatom Substitution to Graphene Nanoribbon. *Sci. Adv.* **2018**, *4*, eaar7181.

24. Nguyen, G. D.; Toma, F. M.; Cao, T.; Pedramrazi, Z.; Chen, C.; Rizzo, D. J.; Joshi, T.; Bronner, C.; Chen, Y.-C.; Favaro, M.; et al. Bottom-Up Synthesis of N = 13 Sulfur-Doped Graphene Nanoribbons. *J. Phys. Chem. C* **2016**, *120*, 2684−2687.

25. Durr, R. A.; Haberer, D.; Lee, Y. L.; Blackwell, R.; Kalayjian, A. M.; Marangoni, T.; Ihm, J.; Louie, S. G.; Fischer, F. R. Orbitally Matched Edge-Doping in Graphene Nanoribbons. *J. Am. Chem. Soc.* **2018**, *140*, 807−813.

26. Carbonell-Sanromà, E.; Garcia-Lekue, A.; Corso, M.; Vasseur, G.; Brandimarte, P.; Lobo-Checa, J.; de Oteyza, D. G.; Li, J. C.; Kawai, S.; Saito, S.; et al. Electronic Properties of Substitutionally Boron-Doped Graphene Nanoribbons on a Au(111) Surface. *J. Phys. Chem. C* **2018**, *122*, 16092−16099.

27. Cai, J.; Pignedoli, C. A.; Talirz, L.; Ruffieux, P.; Söde, H.; Liang, L.; Meunier, V.; Berger, R.; Li, R.; Feng, X.; et al. Graphene Nanoribbon Heterojunctions. *Nat. Nanotechnol.* **2014**, *9*, 896−900.

28. Chen, Y. C.; Cao, T.; Chen, C.; Pedramrazi, Z.; Haberer, D.; de Oteyza, D. G.; Fischer, F. R.; Louie, S. G.; Crommie, M. F. Molecular Bandgap Engineering of Bottom-Up Synthesized Graphene Nanoribbon Heterojunctions. *Nat. Nanotechnol.* **2015**, *10*, 156−160.
29. Bronner, C.; Durr, R. A.; Rizzo, D. J.; Lee, Y. L.; Marangoni, T.; Kalayjian, A. M.; Rodriguez, H.; Zhao, W.; Louie, S. G.; Fischer, F. R.; et al. Hierarchical On-Surface Synthesis of Graphene Nanoribbon Heterojunctions. *ACS Nano* **2018**, *12*, 2193−2200.
30. Jacobse, P. H.; Kimouche, A.; Gebraad, T.; Ervasti, M. M.; Thijssen, J. M.; Liljeroth, P.; Swart, I. Electronic Components Embedded in a Single Graphene Nanoribbon. *Nat. Commun.* **2017**, *8*, 119.
31. Nguyen, G. D.; Tsai, H. Z.; Omrani, A. A.; Marangoni, T.; Wu, M.; Rizzo, D. J.; Rodgers, G. F.; Cloke, R. R.; Durr, R. A.; Sakai, Y.; et al. Atomically Precise Graphene Nanoribbon Heterojunctions from a Single Molecular Precursor. *Nat. Nanotechnol.* **2017**, *12*, 1077−1082.
32. Dienel, T.; Kawai, S.; Söde, H.; Feng, X. L.; Müllen, K.; Ruffieux, P.; Fasel, R.; Gröning, O. Resolving Atomic Connectivity in Graphene Nanostructure Junctions. *Nano Lett.* **2015**, *15*, 5185−5190.
33. Li, J. C.; Sanz, S.; Corso, M.; Choi, D. J.; Peña, D.; Frederiksen, T.; Pascual, J. I. Single Spin Localization and Manipulation in Graphene Open-Shell Nanostructures. *Nat. Commun.* **2019**, *10*, 200.
34. Massimi, L.; Ourdjini, O.; Lafferentz, L.; Koch, M.; Grill, L.; Cavaliere, E.; Gavioli, L.; Cardoso, C.; Prezzi, D.; Molinari, E.; et al. Surface-Assisted Reactions toward Formation of Graphene Nanoribbons on Au(110) Surface. *J. Phys. Chem. C* **2015**, *119*, 2427−2437.

35. Schulz, F.; Jacobse, P. H.; Canova, F. F.; van der Lit, J.; Gao, D. Z.; van den Hoogenband, A. Han, P.; Klein Gebbink, R.; Moret, M.; Joensuu, P. M.; Swart, I.; et al. Precursor Geometry Determines the Growth Mechanism in Graphene Nanoribbons. *J. Phys. Chem. C* **2017**, *121*, 2896−2904.

36. Patera, L. L.; Zou, Z. Y.; Dri, C.; Africh, C.; Reppb, J.; Comelli, G. Imaging On-Surface Hierarchical Assembly of Chiral Supramolecular Networks. *Phys. Chem. Chem. Phys.* **2017**, *19*, 24605−24612.

37. Li, J.; Merino-Díez, N.; Carbonell-Sanromà, E.; Vilas-Varela, M.; de Oteyza, D. G.; Peña, D.; Corso, M.; Pascual, J. I. Survival of Spin State in Magnetic Porphyrins Contacted by Graphene Nanoribbons. *Sci. Adv.* **2018**, *4*, eaaq0582.

38. Su, X. L.; Xue, Z. J.; Li, G.; Yu. P. Edge State Engineering of Graphene Nanoribbons. *Nano Lett.* **2018**, *18*, 5744−5751.

39. Venkatramaiah, N.; Firmino, A. D. G.; Paz, F. A. A.; Tomé, J. P. C. Fast Detection of Nitroaromatics Using Phosphonate Pyrene Motifs as Dual Chemosensors. *Chem. Commun.* **2014**, *50*, 9683−9686.

40. Bartels, L.; Meyer, G.; Rieder, K.-H. Controlled Vertical. Manipulation of Single CO Molecules with the Scanning Tunneling. Microscope: A Route to Chemical Contrast. *Appl. Phys. Lett.* **1997**, 71,213−215.

41. Horcas, I.; Fernandez, R.; Gomez-Rodriguez, J.; Colchero, J.; Gomez-Herrero, J.; Baro, A. WSXM: A Software for Scanning Probe Microscopy and a Tool for Nanotechnology. *Rev. Sci. Instrum.* **2007**, *78*, 013705.

42. Kresse, G.; Furthmüller, J. Efficiency of Ab-Initio Total Energy Calculations for Metals and Semiconductors Using a Plane-Wave Basis set. *Comp. Mat. Sci.* **1996**, *6*, 15−50.

43. Kresse, G.; Furthmüller, J. Efficient Iterative Schemes for Ab Initio Total-Energy Calculations Using a Plane-Wave Basis Set. *Phys. Rev. B* **1996**, *54*, 11169.
44. Klimeš, J.; Bowler, D.; Michaelides, A. Chemical Accuracy for the Van der Waals density Functional. *J. Phys.: Condens. Matter* **2010**, *22*, 022201.
45. Klimeš, J.; Bowler, D.; Michaelides, A. Van Der Waals Density Functionals Applied to Solids. *Phys. Rev. B* **2011**, *83*, 195131.
46. Grimme, S.; Antony, J.; Ehrlich, S.; Krieg, H. A Consistent and Accurate Ab Initio Parametrization of Density Functional Dispersion Correction (DFT-D) for the 94 Elements H-Pu. *J. Chem. Phys.* **2010**, *132*, 154104.
47. Tkatchenko, A.; Scheffler, M. Accurate Molecular Van der Waals Interactions from Ground-State Electron Density and Free-Atom Reference Data. *Phys. Rev. Lett.* **2009**, *102*, 073005.
48. Heyd, J.; Scuseria, G.; Ernzerhof, M. Hybrid Functionals Based on a Screened Coulomb Potential. *J. Chem. Phys.* **2003**, *118*, 8207−8215.
49. Paier, J.; Marsman, M.; Hummer, K.; Kresse, G.; Gerber, I.; Ángyán, J. Screened Hybrid Density Functionals Applied to Solids. *J. Chem. Phys.* **2006**, *124*, 154709.
50. Blöchl, P. E. Projector Augmented-Wave Method. *Phys. Rev. B* **1994**, *50*, 17953.
51. Vanpoucke, D. E. P.; Brocks, G. Formation of Pt-Induced Ge Atomic Nanowires on Pt/Ge(001): A Density Functional Theory Study. *Phys. Rev. B* **2008**, *77*, 241308.
52. Tersoff, J.; Hamann, D. R. Theory of the Scanning Tunneling Microscope. *Phys. Rev. B* **1985**, *31*, 805−813.
53. Humphrey, W.; Dalke, A.; Schulten, K. VMD: Visual Molecular Dynamics. *J. Molec. Graphics* **1996**, *14*, 33−38.

54. Temirov, R.; Soubatch, S.; Neucheva, O.; Lassise, A. C.; Tautz, F. S. A Novel Method Achieving Ultra-High Geometrical Resolution in Scanning Tunneling Microscopy. *New J Phys.* **2008**, *10*, 053012.

55. Gross, L.; Mohn, F.; Moll, N.; Liljeroth, P.; Meyer, G. The Chemical Structure of a Molecule Resolved by Atomic Force Microscopy. *Science* **2009**, *325*, 1110−1114.

56. Hapala, P.; Kichin, G.; Wagner, C.; Tautz, F. S.; Temirov, R. Mechanism of High-Resolution STM/AFM Imaging with Functionalized Tips. *Phys. Rev. B* **2014**, *90*, 085421.

57. Ruffieux, P.; Cai, J. M.; Plumb, N. C.; Patthey, L.; Prezzi, D.; Ferretti, A.; Molinari, E.; Feng, X. L.; Müllen, K.; Pignedoli, C. A.; et al. Electronic Structure of Atomically Precise Graphene Nanoribbons. *ACS Nano* **2012**, *6*, 6930−6935.

58. Cao, T.; Zhao, F. Z.; Louie, S. G. Topological Phases in Graphene Nanoribbons: Junction States, Spin Centers, and Quantum Spin Chains. *Phys. Rev. Lett.* **2017**, *119*, 076401.

59. Gröning, O.; Wang, S. Y.; Yao, X. L.; Pignedoli, C. A.; Barin, G. B.; Daniels, C.; Cupo, A.; Meunier, V.; Feng, X. L.; Narita, A.; et al. Engineering of Robust Topological Quantum Phases in Graphene Nanoribbons. *Nature* **2018**, *560*, 209−213.

60. Rizzo, D. J.; Veber, G.; Cao, T.; Bronner, C.; Chen, T.; Zhao, F. Z.; Rodriguez, H.; Louie, S. G.; Crommie, M. F.; Fischer, F. R. Topological Band Engineering of Graphene Nanoribbons. *Nature* **2018**, *560*, 204−208.

TOC Graphic